COMPARISON BETWEEN EDDY-CORRELATION AND INERTIAL DISSIPATION METHODS IN THE MARINE ATMOSPHERIC SURFACE LAYER

ANNA SJÖBLOM* and ANN-SOFI SMEDMAN

Department of Earth Sciences, Meteorology, Uppsala University, Villavägen 16, SE-752 36 Uppsala, Sweden

(Received in final form 10 December 2002)

Abstract. A comparison of momentum fluxes determined by the eddy-correlation method (ECM) and the inertial dissipation method (IDM) has been performed using long term measurements over the sea. The measurements were made on the island of Östergarnsholm in the middle of the Baltic Sea. The results show that a 'classical' form of the inertial dissipation method, i.e., assuming that the transport terms are negligible, and using an effective value for the Kolmogorov constant of 0.55, can be used with a mean relative difference between the two methods of about 15% for $-1 < z/L < 0.5$ (z being height and L the Obukhov length). The IDM method works best for high wind speeds and neutral conditions. For low wind speeds ($U < 6$ m s^{-1}) the relation between the two methods is more complex. IDM then gives higher values than ECM on the average (about 20%), especially for swell conditions, indicating the need for an imbalance function in the turbulent kinetic energy budget. Calculations of the effective Kolmogorov constant, α_a, suggest a dependence upon the wave age, α_a increasing with increasing wave age, where the value 0.59 fits the data well for saturated waves.

Keywords: Effective Kolmogorov constant, Inertial dissipation method, Marine atmospheric surface layer, Waves.

1. Introduction

Measurements of turbulent fluxes are much more difficult to perform over sea than over land. Mainly two types of measurements are currently used; measurements from fixed masts using the eddy-correlation method, and measurements from ships using the so-called 'inertial dissipation method'. Both strategies have their advantages and disadvantages.

The eddy-correlation method (hereinafter referred to as ECM) is the most direct way to determine the fluxes, but it requires negligible flow distortion and a stable platform, or a moving platform with a motion compensation package. Most studies of this kind have thus been performed at coastal sites, thereby raising the question of the effects of limited water depth and shoaling waves. The inertial dissipation method (hereinafter referred to as IDM) on the other hand is suitable for measurements on moving ships and buoys, since it is less sensitive to motions caused by the ship or buoy and also to flow distortion. The disadvantages is that it relies on

* E-mail: Anna.Sjoblom@met.uu.se

Boundary-Layer Meteorology **110:** 141–164, 2004.

several assumptions that have to be verified if the method is to be used during all conditions.

Some attempts to compare ECM and IDM have been performed earlier, the most thorough comparison up till now being probably the one performed during the HEXOS experiment in the North Sea (e.g., Katsaros et al., 1987; Smith et al., 1992; DeCosmo et al., 1996). The results for IDM gave an uncertainty of 10% for stress, 20% for the sensible heat flux and 25% for the latent heat flux (Fairall et al., 1990). Large and Pond (1981) also compared the two methods using measurements from a site outside Nova Scotia and found that there was good agreement between them.

How waves influence the turbulence structure in the near-surface atmosphere has been a much debated question over the years. Several studies have shown that swell (waves travelling faster than the wind) alter the turbulence structure of the marine atmospheric boundary layer (e.g., Smedman et al., 1999). Whether IDM takes the wave influence into account is one of the most controversial questions associated with that method. Drennan et al. (1999) compared measurements of drag coefficients calculated with IDM and ECM, and found that the measurements made with ECM showed a sea-state dependence, while those made with IDM did not. This was also found by Donelan et al. (1997); in pure wind sea conditions the agreement with ECM was excellent, but during swell IDM was unreliable. Donelan et al. (1997) also showed that flux measurements with ECM gave approximately twice the calculated fluxes compared to IDM when strong swell was present.

Rieder and Smith (1998) suggested a possible explanation for the wave related difference between IDM and ECM. They showed that the inertial subrange does not react in the same way as the low-frequency part of the spectrum, and that most of the swell influence is contained in frequencies between 0.06–0.16 Hz. The inertial subrange is usually located at higher frequencies. Hence, if we measure in the high frequency part of the inertial subrange, it may not be certain that there is any influence of swell at that frequency. IDM might therefore not show a wave influence since it only uses measurements from the inertial subrange, while ECM uses measurements over a much wider range of frequencies.

Another problem with IDM is that it relies on the correct parameterisation of all the terms in the turbulent kinetic energy (TKE) budget. In Sjöblom and Smedman (2002) it was shown that the commonly assumed balance between production and dissipation is questionable during some conditions, and that the different terms depend not only on stability, which has been previously suggested, but also on wave age and to some extent wind speed. IDM also assumes a positive value of the total stress (τ), which is not always the case during swell conditions (Grachev and Fairall, 2001).

The so-called ‘bulk aerodynamical method’ can also be used to calculate fluxes over sea, where only mean meteorological values are needed. With this method, unlike IDM where only the ‘apparent’ wind speed (i.e., the flow past the sensor) is needed, the wind speed has to be determined more carefully. Uncertainties regarding this method also include the numerical value of the drag coefficient C_D. Many attempts have been made to determine C_D, and it is clear that there is a wind speed dependence on C_D (Large and Pond, 1981; Anderson, 1993), but many authors also suggest that there is a wave influence (e.g., Maat et al., 1991; Bergström and Smedman, 1994; Drennan et al., 1999).

This investigation involves a comparison of momentum fluxes determined by IDM and ECM, using long term measurements from a site in the middle of the Baltic Sea called Östergarnsholm. A dataset with more than 900 30-min averages, which all contain wave data, has been used.

As discussed in Sjöblom and Smedman (2002), most of the swell encountered at Östergarnsholm is produced in the southern part of the Baltic Sea and then propagated northwards. Unlike the open ocean where swell originates from several directions, the swell observed at Östergarnsholm is more unidirectional since the Baltic Sea is semi-enclosed. It must therefore be kept in mind that the conditions concerning the effect of swell may be different in the open ocean.

Section 2 describes the measurements, and in Section 3 some theoretical considerations are made. Section 4 describes the data and the calculations, Section 5 gives the results of the comparison between IDM and ECM, and the conclusions are given in Section 6.

2. Measurements

The small island of Östergarnsholm (2×2 km) is situated about 4 km east of the island of Gotland in the middle of the Baltic Sea (Figure 1). On this island, semi-continuous measurements have been performed on a 30-m tower since May 1995. Östergarnsholm is a very flat island, with only sparse vegetation and no trees.

In Smedman et al. (1999) the possible influence of a limited water depth on the tower measurements was studied in detail. Flux footprint calculations were done, showing that the turbulence instruments 'see' areas far upstream of the island. Sufficiently long waves 'feel' the presence of the bottom, implying that the peak wave phase speed c_0 must be calculated using the dispersion relation

$$c_0 = \frac{g}{\omega_0} \tanh\left(\frac{\omega_0 h}{c_0}\right). \qquad (1)$$

Taking the 'footprint weighting function' $F(z)$ from Equation (A7) of the Appendix of Smedman et al. (1999), it is possible to calculate a weighted mean phase speed

$$\langle c_0 \rangle = \int_0^\infty F(x, z) c_0(x)\, \mathrm{d}x. \qquad (2)$$

In Smedman et al. (1999) it was found that, although the phase speed of the relatively long waves was indeed influenced by shallow water effects, little or no effect

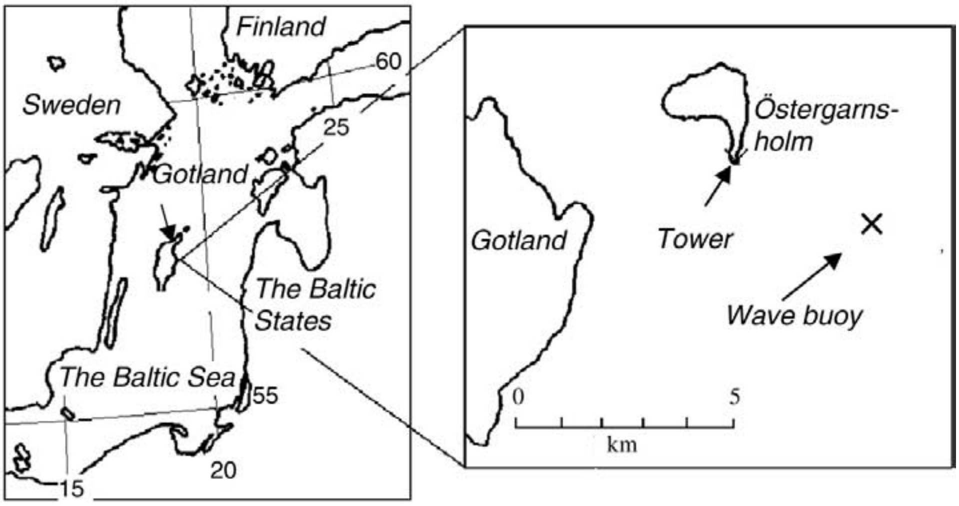

Figure 1. Map of the Baltic Sea, with a close up on Östergarnsholm. The location of the wave buoy is also indicated.

of wave steepness was observed. A comparison was done with the case of Anctil and Donelan (1996) and it was concluded that for gale conditions "we do not expect the shallow-water effects at our lowest level to be as strong as those observed by Anctil and Donelan".

A comparison for some of the data used in this study of c_0 calculated with Equation (2), and an equivalent calculated c_0 using the deep water relationship, showed only a slight influence on individual values, and no significant difference on the averaged values. Therefore, only a small correction based on this comparison has been applied for the highest wind speeds.

The base of the tower is situated at about 1 m above sea level. In the sector 100°–220° the water fetch is undisturbed, and the distance to the shoreline in this direction is normally no more than a few tens of metres. Östergarnsholm will therefore represent open sea conditions of the Baltic Sea for most of the time when the wind is from the sector 100°–220°.

The actual height from the water level to the instruments on the tower fluctuates due to varying sea level. Corrections for varying sea levels were performed with the aid of sea-level measurements in Visby harbour on the west coast of Gotland. For more details, see Sjöblom and Smedman (2002). For the data used, the height above the water to the lowest turbulence instrument (9 m above tower base) will vary between 10.0 m and 10.7 m, with an average of 10.4 m.

Turbulence instruments (Solent Ultrasonic Anemometer 1012R2, Gill Instruments, Lymington, United Kingdom) are placed at 9, 17 and 25 m above the tower base and data recorded at 20 Hz. Slow response ('profile') instruments are placed at five heights on the tower, at 7, 12, 14, 20 and 29 m above the tower base, measuring wind speed, wind direction and temperature at 1 Hz.

The calibration procedure for the sonic anemometers follows that of Grelle and Lindroth (1994), where the flow distortion made by the instrument itself is taken into account in a calibration matrix. From this the three wind components are obtained. The sonic anemometers and also the light weight cup anemometers were individually calibrated in a large wind tunnel before they were installed on the tower.

The temperature measured by the sonic anemometers T_s is very close (about 0.20%) to the virtual temperature T_v (Dupuis et al., 1997; Sjöblom and Smedman, 2002). The virtual heat flux $\overline{w'\theta_v'}$ has been corrected for 'cross-wind' velocity contamination, since the signal is contaminated by the wind components normal to and along the path (Kaimal and Gaynor, 1991). However, this correction is based on a vertical orientation of the sonic temperature sensor, which is not the case for the sonic used here. How large an error this difference gives is not clear, but it has been shown that the results are substantially improved when the correction is applied (C. Johansson, personal communication, 2002).

In addition to the tower instruments, a Wave-Rider Buoy (owned and run by the Finnish Institute of Marine Research) is deployed about 4 km from Östergarnsholm (direction 115°, Figure 1). The buoy is moored at 36 m water depth, and it is placed upwind of the measurements, thereby representing the wave conditions in the 'footprint area' outside Östergarnsholm. It measures sea surface (bucket) temperature, significant wave height, wave direction and the energy spectra of the wave field.

Wave data are recorded once an hour, and the directional spectrum is calculated from 1600 s of data onboard the buoy; the spectrum has 64 frequency bands (0.025–0.58 Hz). The significant wave height is calculated by a trapezoidal method from frequency bands in the range 0.05–0.58 Hz, and the peak frequency is determined by a parabolic fit (Smedman et al., 1999). The wave measurements have been performed semi-continuously during the same period as the tower measurements with the exception of wintertime periods with risk for ice damage.

3. Theory

3.1. The Eddy-Correlation Method

The most direct way to determine the fluxes is to use the so-called eddy-correlation method, where the correlation between the fluctuations is determined directly, and the total stress, τ can be calculated,

$$\tau = -\rho|\boldsymbol{i}\overline{u'w'} + \boldsymbol{j}\overline{v'w'}| = \rho u_*^2, \tag{3}$$

where $\overline{u'w'}$ and $\overline{v'w'}$ are the components of the kinematic momentum flux in the along-wind ($\boldsymbol{i}$) and cross-wind ($\boldsymbol{j}$) directions, ρ the air density, and u_* is the friction velocity, which, according to Equation (3), can be computed from:

$$u_*^2 = [(-\overline{u'w'})^2 + (-\overline{v'w'})^2]^{1/2}. \tag{4}$$

Over the land, this method is obviously the best choice, but on a moving ship or buoy corrections have to be made. These involve both the motion of the ship or buoy, which is in the same frequency interval as that contributing to the flux itself, and possible flow distortion effects need to be accounted for (e.g., Edson et al., 1991; Oost et al., 1994; Yelland et al., 1998).

However, there are some studies where the necessary corrections have been successfully applied to ECM measurements performed on ships and buoys (e.g., Anctil et al., 1994; Edson et al., 1998). Unfortunately this has been quite an expensive method and the flow distortion has to be known for every individual ship or buoy. IDM might therefore still be easier to use on ships and buoys and will be discussed below.

3.2. The Inertial Dissipation Method

In the inertial dissipation method, the friction velocity u_* (Equation (4)) is determined with the aid of the normalised TKE budget, which during stationary and horizontally homogeneous conditions is defined as

$$\underset{(PN)}{\frac{kz}{u_*^3}\left(\overline{u'w'}\frac{\partial\bar{u}}{\partial z}\right)} - \underset{(BN)}{\frac{kz}{u_*^3}\frac{g}{T_0}\overline{w'\theta_v'}} + \underset{(T_tN)}{\frac{kz}{u_*^3}\frac{\partial\overline{w'e}}{\partial z}} + \underset{(T_pN)}{\frac{kz}{u_*^3}\left(\frac{1}{\rho}\right)\frac{\partial\overline{p'w'}}{\partial z}} + \underset{(DN)}{\frac{kz}{u_*^3}\epsilon} = 0, \tag{5}$$

which can be written as,

$$\underset{(PN)}{\phi_m} - \underset{(BN)}{\frac{z}{L}} - \underset{(T_tN)}{\phi_t} - \underset{(T_pN)}{\phi_p} - \underset{(DN)}{\phi_\epsilon} = 0, \tag{6}$$

where $e = 0.5(u'^2 + v'^2 + w'^2)$. Term (PN) corresponds to the normalised mechanical production of TKE from the mean flow, (BN) is the normalised buoyant production or loss, (T_tN) is the normalised turbulent transport, (T_pN) is the normalised pressure transport and (DN) is the normalised molecular dissipation of TKE. $\overline{w'\theta_v'}$ is the flux of virtual potential temperature, T_0 is a reference temperature in the surface layer, k is the von Karman constant, g the acceleration due to gravity, z is the height of the measurements and L is the Obukhov length, defined by

$$L = -\frac{u_*^3 T_0}{gk\overline{w'\theta_v'}}. \tag{7}$$

The dissipation, ϵ, can be determined from the inertial subrange of velocity spectra by assuming Kolmogorov similarity, and applying Taylor's hypothesis

$$DN = -\phi_\epsilon = -\frac{\epsilon kz}{u_*^3} = -\frac{kz}{u_*^3}\left[\frac{nS_u(n)}{\alpha}\right]^{3/2}\left(\frac{2\pi}{u_{\text{apparent}}}\right)n, \tag{8}$$

where α is the Kolmogorov constant, n the frequency in Hz, $S_u(n)$ is the spectral intensity and u_{apparent} is the apparent wind speed, which is equal to the wind speed measured at a fix point on a moving ship. The ϕ functions of Equation (6) are normally assumed to be functions only of z/L. A more thorough description of the TKE budget and all the terms is given in Sjöblom and Smedman (2002). Solving for u_* in Equation (8), and using Equation (6), gives

$$u_*^3 = \left[\frac{nS_u(n)}{\alpha}\right]^{3/2}\left(\frac{2\pi}{u_{\text{apparent}}}\right)\left(\frac{kz}{\phi_m - z/L - \phi_t - \phi_p}\right)n. \tag{9}$$

Equation (3) can then be rewritten together with (9) in the form

$$|\tau| = \rho u_*^2 = \rho\left(\left[\frac{nS_u(n)}{\alpha}\right]^{1/2}\left[\left(\frac{2\pi}{u_{\text{apparent}}}\right)\left(\frac{kz}{\phi_m - z/L - \phi_t - \phi_p}\right)n\right]^{1/3}\right)^2. \tag{10}$$

However, there are some problems involved in this procedure. To calculate u_* from Equation (9), the stability z/L is needed (Equation (7)), and to calculate z/L u_* must be known. So to determine u_* from the ϕ functions, which are defined as functions of z/L, either an independent estimation of z/L has to be made, or an iterative calculation is needed.

The iterative process is often used, assuming neutral stability as a starting value, and then iterations are performed until convergence is achieved. Dupuis et al. (1997) find that this iterative method gives a low rate of convergence and that some other procedure should be used. They applied two other methods; firstly the buoyancy flux $\overline{w'\theta_v'}$ is determined by a bulk estimation using averaged values for air temperature, specific humidity and sea surface temperature. The second method includes dissipation rates for wind and virtual temperature in each step.

A method where no iteration at all is necessary was introduced by Large and Pond (1982), where an estimation of z/L was made with a bulk formulation using only mean values of wind speed, specific humidity and air–sea temperature difference. The ϕ functions and u_* can then be calculated directly using this z/L value.

Taylor and Yelland (2000) also discuss an approach to calculate z/L and u_* without iterations. An estimation of z/L was first made with a bulk value of u_* calculated from mean meteorological values. This z/L value could then be used to calculate a new value of the friction velocity u_* (Equation (9)), thereby avoiding a possible problem with iterations.

It is common to assume that the transport terms are small or equal in magnitude, i.e., that local production equals local dissipation (e.g., Large and Pond, 1981; Edson et al., 1991). This is however not always the case. In Sjöblom and Smedman (2002) it was shown that the imbalance depends on the stability, wind speed and also on wave conditions. The wave influence will be discussed more in the next section.

3.3. Waves

The wave age is one way to describe the development of the wave field; it may be defined as,

$$\text{Wave age} = c_0/(U_{10}\cos\theta), \tag{11}$$

where c_0 is the phase velocity of the waves at the peak of the spectrum, U_{10} the wind speed at 10 m and θ the angle between wind and wave directions. Swell is here defined as $c_0/(U_{10}\cos\theta) > 1.2$ (Pierson and Moskowitz, 1964). An alternative definition of wave age is

$$\text{Wave age} = c_0/u_* \tag{12}$$

and swell is then defined as $c_0/u_* > 30$ (Volkov, 1970).

The total stress (Equation (3)) can be divided into three parts

$$\tau = \tau_{\text{turb}} + \tau_{\text{wave}} + \tau_{\text{visc}}, \tag{13}$$

where τ_{turb} is the turbulent shear stress, τ_{wave} the wave induced stress and τ_{visc} the viscous stress. For swell, τ_{wave} will be negative, and therefore it reduces the total stress; values close to zero, or even with reversed sign, are not uncommon (e.g., Smedman et al., 1994; Grachev and Fairall, 2001). This will then of course also affect the friction velocity u_* (Equation (3)), and thereby the stability expressed as z/L (Equation (7)). Contrary to the case over land, it is u_* rather than the heat flux $\overline{w'\theta_v'}$ that most influences the stability, since the heat flux is often small and varies little. As discussed in Sjöblom and Smedman (2002), u_* can become very small during swell conditions, thereby inducing large values of $|z/L|$, even if the heat flux is small. Thus, there is a close connection between wave age and stability.

The wave age and the wind speed are also related, and swell is usually associated with low wind speeds. However, in this study, a swell component can be seen at as high wind speed as 10 m s^{-1}.

4. Data and Calculations

The dataset consists of 922 30-min averages with ECM and IDM data. Measurements are taken from the period May 1995–December 1997, and only those with long (more than 150 km) overwater fetch, and only data with corresponding wave information, have been used. The wind speed ranges from 2 to 18 m s^{-1}; data with wind speeds less than 2 m s^{-1} have been removed due to statistical uncertainties. The stability ranges from very unstable to stable $-10 < z/L < 0.5$, even though most of the data fall in the near-neutral range (more than 95% lies between $-1.0 < z/L < 0.5$). Data with more than an 80° difference between the wave and wind directions have been removed. The data show hardly any dependence on the choice of this angle (using, for example, 40° does not change the results significantly). Of the total dataset, 369 values are characterised as swell.

The dissipation rate was determined from manually checked spectra of longitudinal wind velocity, with spectra first averaged into logarithmic bins of frequency n (in Hz), with five average values for each decade in frequency. When the slope of a log–log fit of four adjacent points in the inertial subrange was approximately $-2/3$, values of $nS_u(n)$ and n were calculated from this curve ($n \sim 1$ Hz), and then used both for the ECM and IDM calculations. Spectra that did not fulfil the above requirements have been rejected.

The manual check was necessary since the inertial subrange shifts along the frequency axis due to varying wind speeds, and it is also a way to avoid problems with high frequency noise. Both problems might exist if the averaging is performed automatically.

Two different methods of calculations for IDM have been used: One is from the Southampton Oceanography Centre (SOC) (e.g., Taylor and Yelland, 2000) and the other from the Centre d'Etude des Environnements Terrestres et Planetaires (CETP) (e.g., Dupius et al., 1997). A method with no iterations was used for the calculations, i.e., the stability z/L was estimated from a bulk value of u_*.

The calculations follow that of Taylor and Yelland (2000), where a bulk value of the drag coefficient C_D has been determined from the measured wind speed and the difference between air and water temperatures (e.g., Smith, 1988; Josey et al., 1999). The friction velocity, u_*, can then be calculated from the definition of C_D

$$C_D = \left(\frac{u_*}{U}\right)^2. \tag{14}$$

Since a direct estimate of the virtual heat flux $\overline{u'\theta_v'}$ is uncommon when IDM is used, bulk formulations are used instead

$$\overline{w'\theta_v'} = \overline{w'\theta'} + 0.61T_0\overline{w'q'}, \tag{15}$$

where

$$\overline{w'\theta'} = C_H U(T_s - T_z) \tag{16}$$

and

$$\overline{w'q'} = C_E U(q_s - q_z). \tag{17}$$

Here, T_s is the sea surface temperature, q_s the specific humidity at the sea surface and q_z the specific humidity at the measuring height. The exchange coefficients C_H and C_E are taken as 1.0×10^{-3} and 1.2×10^{-3} respectively (Smith, 1988).

The stability z/L can now be calculated, as

$$\frac{z}{L} = -\frac{zgk\overline{w'\theta_v'}}{u_*^3 T_0} \tag{18}$$

and hence the normalised wind gradient, ϕ_m, using

$$\phi_m = (1 - 16z/L)^{-1/4} \qquad z/L < 0, \tag{19a}$$

$$\phi_m = 1 + 5z/L. \qquad z/L > 0. \tag{19b}$$

The IDM value of the friction velocity u_* is then calculated with the assumption of zero imbalance in Equation (9) (i.e., $-\phi_t - \phi_p = 0$), which gives

$$u_* = \left[\frac{nS_u(n)}{\alpha}\right]^{1/2} \left[\left(\frac{2\pi}{U}\right) \frac{kzn}{(\phi_m - z/L)}\right]^{1/3}. \tag{21}$$

In the above, α was set to 0.55 and k to 0.40; $nS_u(n)$, n, z and U are the same as used in the ECM calculations.

5. Results

The difference between the results from the two IDM algorithms was very small, with the correlation coefficient greater than 0.99, and a standard deviation of 0.11. Therefore, in the following section, only the results from the SOC method will be used.

5.1. The stability parameter z/L

The stability parameter z/L was determined from Equation (7) for ECM calculations, using T_0 from the profile measurements, with cross-wind corrected heat flux from the sonic anemometer. k, is set equal to 0.40, according to Högström (1996). These z/L values were then compared to those obtained from the IDM calculations.

In Figure 2, a comparison of z/L calculated with ECM and IDM is shown. Figure 2a shows all data, and Figure 2b a close up of the near-neutral values. The

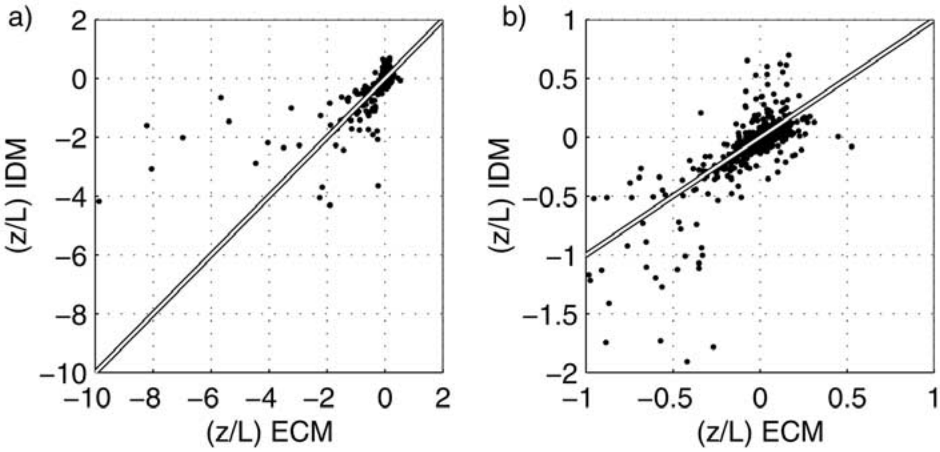

Figure 2. The stability parameter z/L from the eddy-correlation method (ECM) and the inertial dissipation method (IDM). Filled circles (●) are the measurements: (a) All data, (b) a close up of data between $-1 < z/L < 1$.

TABLE I

Correlation coefficients and standard deviations for the stability z/L determined by IDM and EC.

Stability	Number of data	Correlation coefficient	Bias	Standard deviation
All data ($-10 < z/L < 0.5$)	922	0.71	−0.05	0.71
Near neutral ($-1 < z/L < 0.5$)	889	0.69	−0.02	0.16
Unstable ($z/L < -2$)	14	0.10	−2.12	2.42

correlation coefficients, biases and standard deviations between the two methods for different stability ranges are given in Table I. The correlation coefficient for $-1 < z/L < 0.5$ is 0.69, while for $z/L < -2$ it is as low as 0.10. It can however be noted that the bias is negative in all the stability ranges, i.e., IDM gives lower values of $|z/L|$ than ECM on the average.

For very unstable cases (calculated with ECM, Figure 2a), IDM gives more neutral values than ECM. Here the wind speed is usually low and practically all values are influenced by swell. These smaller $|z/L|$ values are probably an effect of small u_* related to the influence of waves (discussed in Section 3), a phenomenon not completely captured using IDM. Also, it is possible that the bulk formulation of z/L in the IDM is inaccurate during unstable conditions (Dupuis et al., 1997). But, as seen in the Figure, there are only 14 points in the interval $z/L < -2$, and

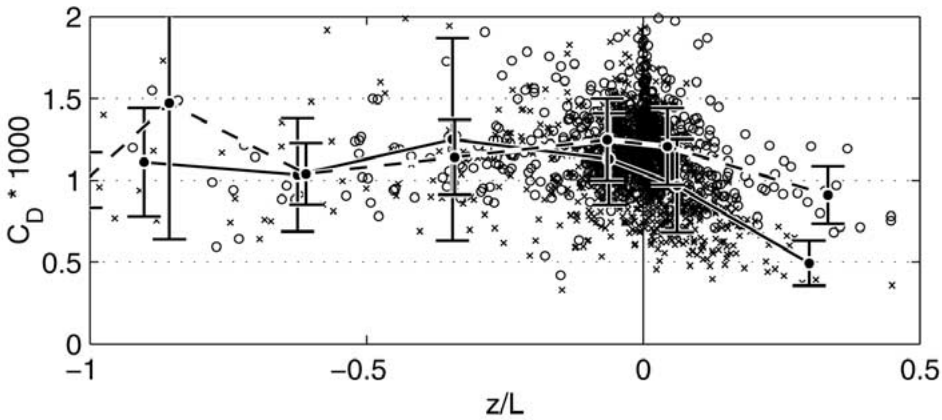

Figure 3. The drag coefficient as a function of the stability z/L, from the ECM, solid line (—), and IDM, dashed line (- -). z/L has been determined with separate methods, as described in the text. Crosses ($\times$) are ECM and open circles ($\bigcirc$) IDM. The filled circles ($\bullet$) show bin-averaged values with standard deviations.

as said above most data are in the stability range $-1 < z/L < 0.5$. Therefore only data with $-1 < z/L < 0.5$ will be used henceforth.

For this stability interval, shown in Figure 2b, the agreement between the two methods is better, but there are some large deviations for larger $|z/L|$ values. However, there are of course some uncertainties regarding the exact value of z/L, or rather the heat fluxes from the sonic anemometer.

Correctly determined stability is important in calculating u_* (Equation (20)) with IDM, since the stability z/L is used in the ϕ functions and will therefore also influence the calculated u_* values. But it is also important when the drag coefficient C_D is reduced to an effective neutral value, since an erroneous z/L value will give an erroneous calculation.

5.2. THE DRAG COEFFICIENT C_D

The drag coefficient C_D is defined in Equation (14). In Figure 3, averaged curves of C_D from ECM (solid line —) and IDM (dashed line - -) are shown as a function of z/L. Crosses ($\times$) are individual values from ECM and open circles ($\bigcirc$) from IDM; the filled circles ($\bullet$) show bin-averaged values with standard deviations.

Note that as described above, z/L has been determined using different methods for ECM and IDM. Also, it is the C_D value calculated with u_* from IDM (Equation (20)) that is used in Figure 3, *not* the bulk C_D used to determine the stability z/L.

The two methods give similar values for $z/L < -0.1$. For neutral conditions, IDM gives slightly higher values than ECM, but they are still within one standard deviation. The difference between IDM and ECM is more pronounced on the stable side ($z/L > 0$), the difference increasing with increasing z/L.

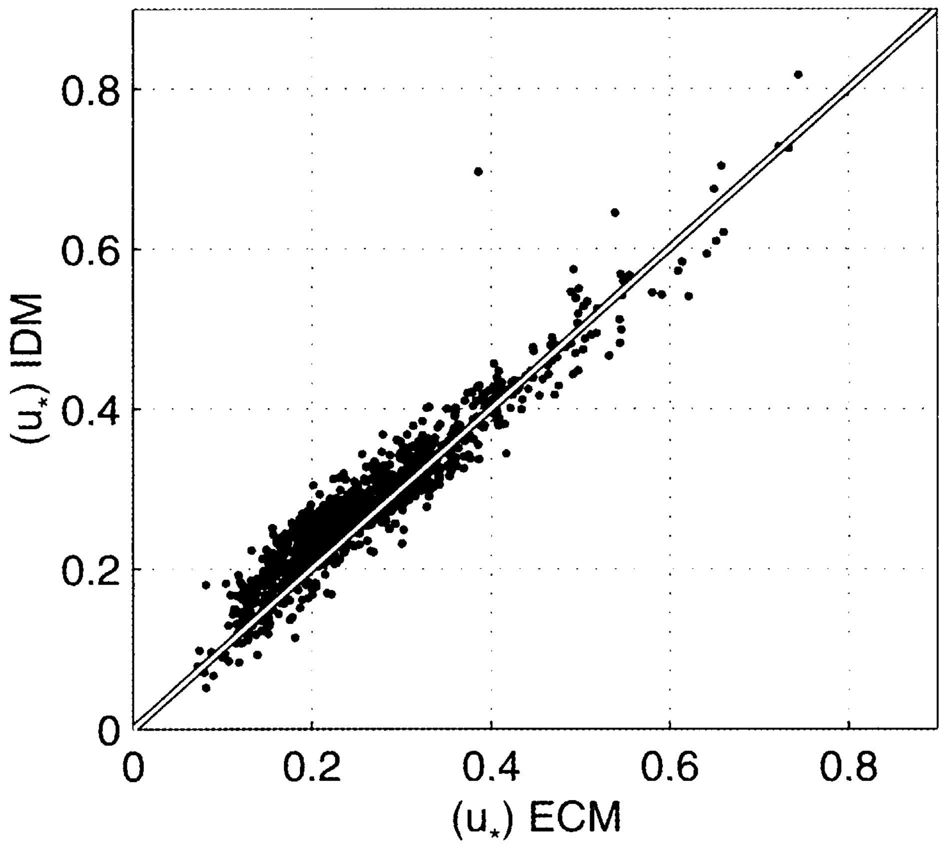

Figure 4. The friction velocity u_* [m s^{-1}] from ECM (x-axis) and IDM (y-axis).

5.3. THE FRICTION VELOCITY u_*

The friction velocity, u_*, is plotted in Figure 4, determined from IDM (y-axis) (Equation (20)) and ECM (x-axis) (Equation (4)).

The agreement between the two methods is fairly good, especially for high values, but for 0.1 m s^{-1} $< u_* <$ 0.4 m s^{-1} IDM has a tendency to give higher values than ECM. The correlation coefficients, the bias and the standard deviations for different u_* ranges are given in Table II. The bias for 0.1 m s^{-1} $< u_* <$ 0.4 m s^{-1} (0.05 m s^{-1}) is more than twice the bias for $u_* >$ 0.4 m s^{-1} (0.02 m s^{-1}), and the bias is positive, i.e., higher IDM than ECM values, on the average.

The stability dependence of the difference between the two methods is illustrated in Figure 5, where the ratio of u_* calculated with IDM and ECM respectively, is plotted as a function of z/L (determined from ECM). The mean relative difference between the two methods is about 15%. On *average*, the two methods agree well for unstable conditions, but as for C_D, IDM gives larger values than ECM

TABLE II

Correlation coefficients and standard deviations for the friction velocity u_* (in m s^{-1}) determined by IDM and EC.

Friction velocity u_*	Number of data	Correlation coefficient	Bias	Standard deviation
All data	889	0.95	0.04	0.11
$0.1 < u_* < 0.4$	787	0.90	0.05	0.07
$u_* > 0.4$	93	0.92	0.02	0.08

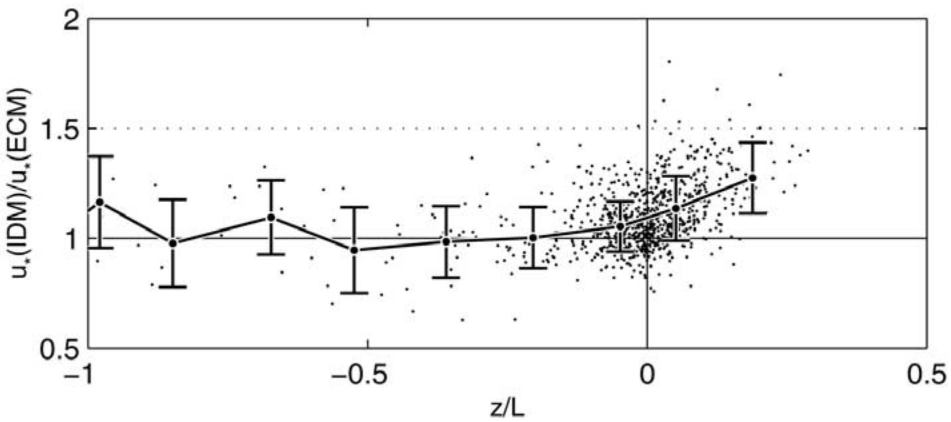

Figure 5. Ratio of u_* from IDM and u_* from ECM as a function of stability, z/L. The dots (·) are the data, the solid line (—) the averaged curve, and the filled circles (●) are the bin-averaged values with error bars.

when moving towards neutral conditions, and during stable conditions IDM gives significantly larger values than ECM.

In Figure 6, the ratio of u_* from IDM and by u_* from ECM is plotted as a function of wind speed (symbols as in Figure 5). Only near-neutral values have been used ($-0.02 < z/L < 0.02$) in an attempt to avoid most of the stability dependence. The mean relative difference between the two methods is now reduced to about 10%.

In Figure 6a, all data are plotted, and above approximately 10 m s^{-1} the agreement between the two methods is good, but also wind speeds above 6 m s^{-1} give acceptable results with a bias of 0.05, i.e., there is a tendency for IDM to give higher values than ECM. By only using data with $c_0/(U_{10} \cos\theta)$ between 0.5–1.0, showed in Figure 6b, thus avoiding much of the swell influence (and thereby also the lowest wind speeds), the bias is 0.03 for wind speeds above 8 m s^{-1}.

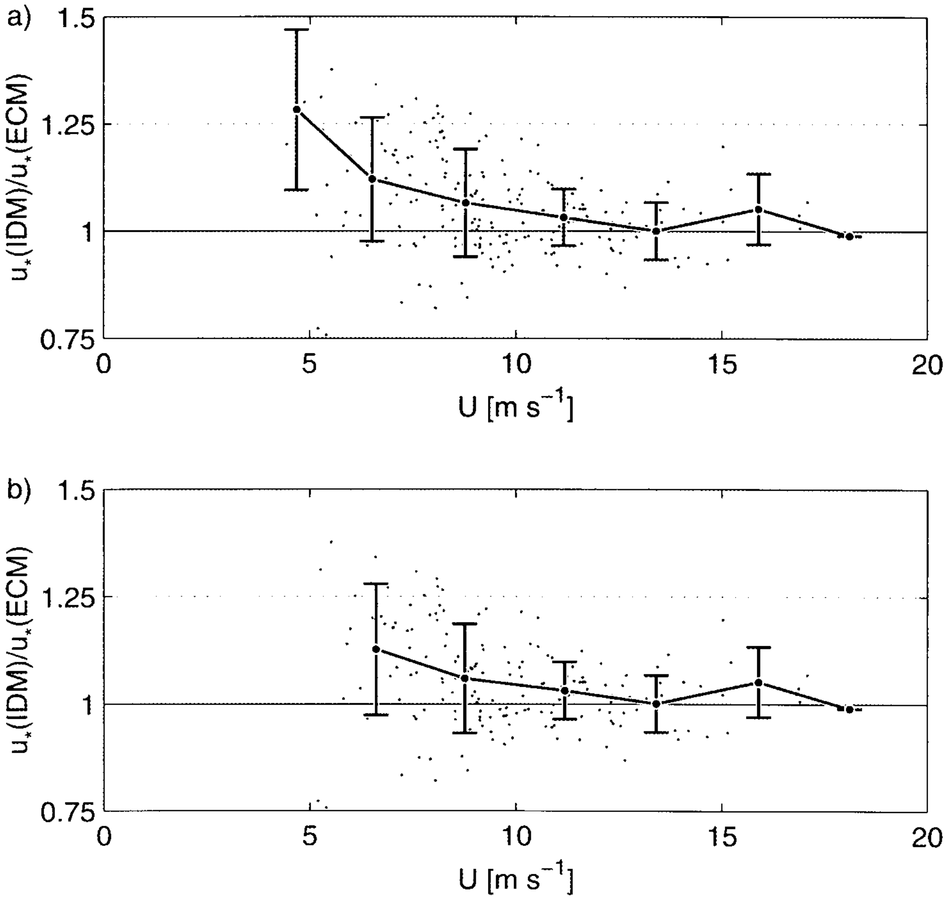

Figure 6. Ratio of u_* from IDM and u_* from ECM as a function of wind speed, symbols as in Figure 5: (a) All data, (b) only data with wave age $0.5 < c_0/(U_{10}\cos\theta) < 1.0$. Near-neutral data $(-0.02 < z/L < 0.02)$.

This can also be seen in Figure 7, where the ratio of u_* between IDM and ECM $(-0.02 < z/L < 0.02)$ is plotted as a function of wave age (symbols as in Figure 5). In Figure 7a, the wave age is defined as $c_0/(U_{10}\cos\theta)$ (Equation (10)), and in Figure 7b as c_0/u_* (Equation (11)). Both figures show a wave-age dependence, the ratio increasing with increasing wave age. Figures 7a and b correspond well with Figure 6, because high wave age is connected with low wind speed and IDM again gives larger values than ECM. This can be compared to Figure 5, where the ratio at neutral conditions was larger than 1.0, i.e., swell and low wind speed influence also at neutral conditions.

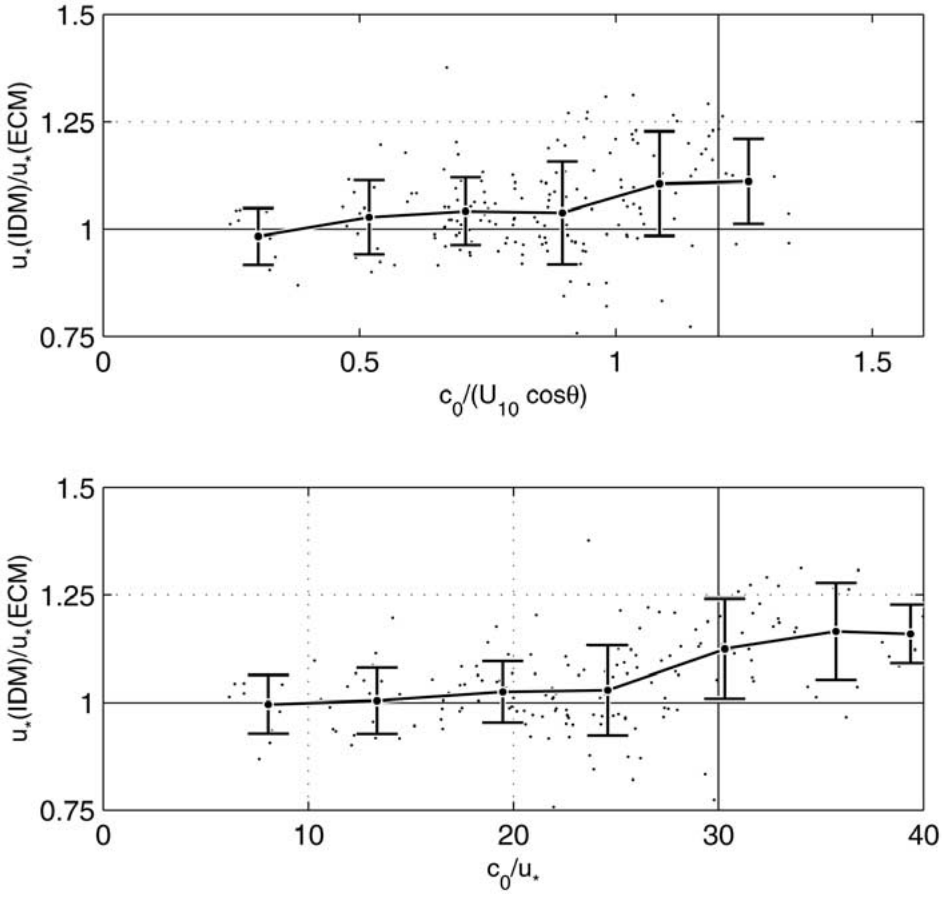

Figure 7. Ratio of u_* from IDM and u_* from ECM plotted as a function of two wave-age estimates: (a) as a function of $c_0/(U_{10}\cos\theta)$, (b) c_0/u_*. Symbols as in Figure 5. Near-neutral data ($-0.02 < z/L < 0.02$).

5.4. Dependence of Correct ϕ Functions

Calculations of u_* with IDM require correct parameterisation of the ϕ functions (Equation (20)). The normalised wind gradient, ϕ_m, over sea differs sometimes considerably from that found over land. In Figure 8, taken from Sjöblom and Smedman (2002), ϕ_m measured at Östergarnsholm is plotted as a function of stability (symbols as in Figure 5). As a comparison, the ϕ_m curve suggested by Högström (1996), which is representative of land conditions, is also shown.

Looking at the near-neutral data, the curve falls off much more rapidly when moving towards convective conditions compared to the curve suggested by Högström (1996). This originates from the shape of the wind profile, since the gradient $(\partial U/\partial z)$ is used to calculate ϕ_m (Equation (5)). Figure 9 shows two typical examples of wind profiles (schematically) during neutral conditions.

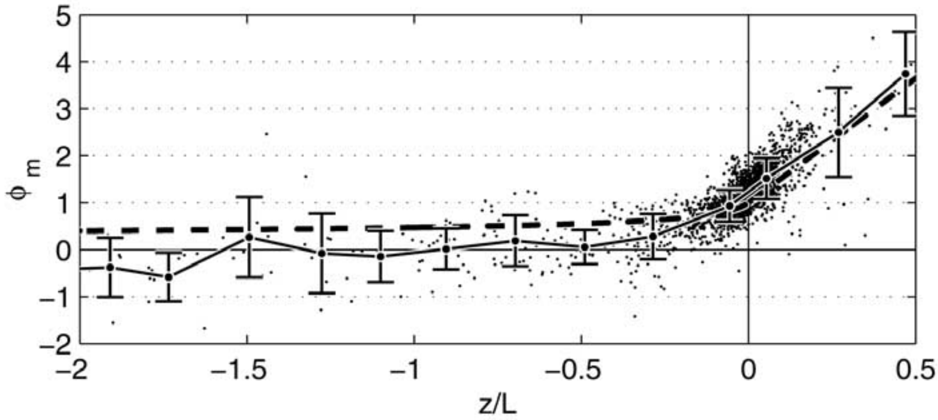

Figure 8. Normalised wind gradient ϕ_m as a function of stability. Symbols as in Figure 5, dashed line (- -) is the curve of Högström (1996). After Sjöblom and Smedman (2002).

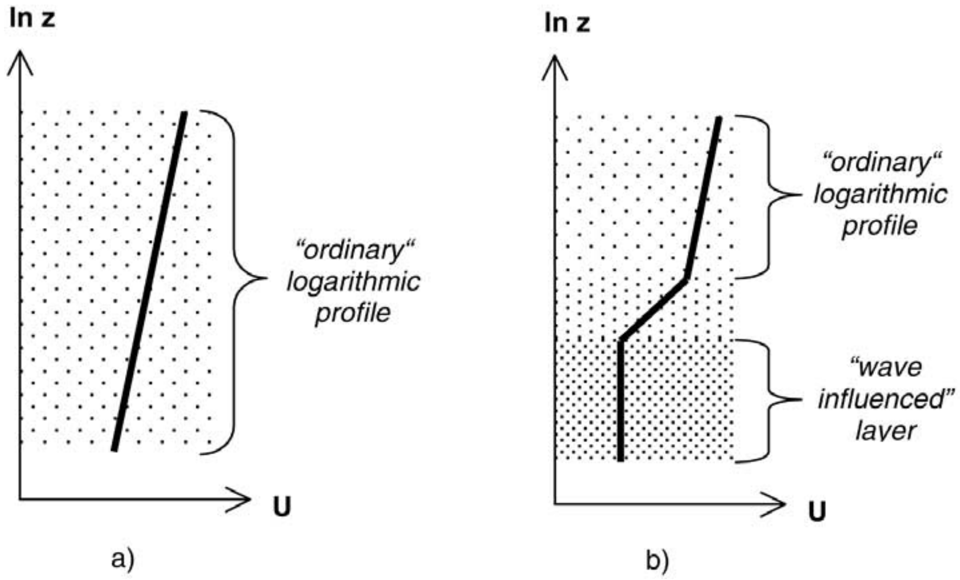

Figure 9. Two typical examples of wind profiles (schematically) during neutral conditions: (a) Growing sea with an 'ordinary' logarithmic profile, (b) swell with a wave influenced layer.

For a growing sea, the wind profile over sea resembles that over land, i.e., it is logarithmic for neutral conditions (Figure 9a).

During swell, a 'wave-driven wind' is not an uncommon feature (Smedman et al., 1999), giving a wind profile more 'straight' than the logarithmic profile. For strong swell cases, the profile might even have a negative slope, giving a very small or even negative gradient in the wave influenced layer (Figure 9b). These small or negative gradients will then give small or negative ϕ_m values (Sjöblom and Smedman, 2002; Sjöblom and Smedman, 2003). And, as discussed in Section 3, unstable data ($z/L < -0.5$) are almost always influenced by swell, thereby having a smaller (or negative) ϕ_m than those determined over land.

Therefore, the ϕ_m used in the IDM calculation (Equation (20)) should be adjusted to sea conditions rather than using a land based curve. The integrated ϕ_m function, used when C_D is recalculated to neutrality, also has to be corrected for sea conditions. Also, ϕ_m occurs in the denominator of Equation (20). If the actual ϕ_m value is much lower than the calculated value (e.g., Equation (19)), this will affect the estimation of u_*, giving a small value. This would explain why Donelan et al. (1997) find that ECM gives larger values than IDM during strong swell situations.

However, in this dataset, there are too few values that are unstable enough to support the findings of Donelan et al. (1997), even if a tendency towards this can be found (not shown). Also, Donelan et al. (1997) had values with swell in the opposite direction from the wind direction, and those have been removed here.

As shown above, IDM gives higher values than ECM during swell. A reason for this is probably the assumption in the IDM that the transport terms are negligible. Another possible cause is that the estimation of the stability, z/L, can be erroneous (Section 5.1), and if $|z/L|$ is smaller than it should be, ϕ_m will be calculated at the wrong stability (Equation (19)).

5.5. Kolmogorov's constant

Several values have been suggested for Kolmogorov's constant α (Equation (8)) over the years. Högström (1990) suggests $\alpha = 0.52$ after a comprehensive review of values reported in the literature, all based on direct estimates of dissipation. This value is also commonly used (e.g., Schacher et al., 1981; Fairall and Larsen, 1986).

Deacon (1988) suggested that instead of an imbalance function (i.e., imbalance $= -\phi_t - \phi_p$) in Equation (10) an *effective* or *apparent* value of Kolomogorov's constant (α_a) could be used to account for a possible imbalance between production and dissipation in the TKE budget. This value will only be equal to the true Kolmogorov constant, α, if the assumption of balance between production and dissipation holds true, i.e., that the sum of the transport terms is negligible. In the above calculations with IDM, a value of $\alpha_a = 0.55$ has been used. This value is widely quoted (e.g., Yelland and Taylor, 1996; Donelan et al., 1997). Large and Pond (1981) used this value and found good agreement between IDM and ECM, especially for neutral conditions. For stable and unstable conditions, the scatter becomes somewhat larger.

Unfortunately, not much has been done earlier regarding a possible wave influence on α_a. The most thorough review of α_a has probably been done by Deacon (1988), who used earlier experiments to calculate α_a both over land and over sea. The range of α_a found in his study is 0.50 to 0.77, with more scatter in the data over sea than over land. Even if the data were presented as averaged values for

TABLE III

Effective Komlogorov constant, α_a, in different wave-age intervals.

Wave-age interval	Number of data	α_a
All data	109	0.59
$c_0/(U_{10}\cos\theta) < 0.5$	10	0.49
$0.5 < c_0/(U_{10}\cos\theta) < 1.2$	86	0.59
$c_0/(U_{10}\cos\theta) > 1.2$	13	0.65
$c_0/u_* < 15$	19	0.50
$15 < c_0/u_* < 30$	69	0.59
$c_0/u_* > 30$	21	0.65

each experiment, a tendency for experiments with high wind speeds (associated with low wave ages) to have lower values of α_a, and those with low wind speeds (associated with high wave ages) to have higher values of α_a, exists. The averaged value of Deacon's study was $\alpha_a = 0.59$ (determined both over land and sea).

Paquin and Pond (1971) calculated α_a over sea using structure functions and skewness, giving an average value $\alpha_a = 0.57$ with a range from 0.52 (one value was 0.32) to 0.75. Also, looking at their individual values (Table 1 of Paquin and Pond, 1971), a trend of increasing α_a with decreasing wind speed can be found. Large values of α_a over sea was also found by van Atta and Chen (1970), with an average of 0.70.

Using only very near-neutral values ($-0.01 < z/L < 0.01$), α_a can be calculated using ECM data. In Figure 10, α_a is plotted as a function of wave age (symbols as in Figure 5). Figure 10a shows α_a as a function of $c_0/(U_{10}\cos\theta)$ and Figure 10b as a function of c_0/u_*. Even if the dataset now has been reduced substantially, it seems as if α_a shows a wave-age dependence, α_a increasing with increasing wave age (a few extreme data points are outside the figures). If the data are divided into three wave-age intervals (young waves, saturated waves and swell), the average values will be as shown in Table III. The overall mean is 0.59, but α_a is smallest for young waves and largest for swell.

Most of the data are representative for saturated waves in the wave-age interval ($0.5 < c_0/(U_{10}\cos\theta) < 1.2$ or $15 < c_0/u_* < 30$), and the average value here is 0.59. This value is similar to that found over land (Högström, 1990), and it also supports the findings of Sjöblom and Smedman (2002) who suggested that the aerodynamic properties of the sea surface in this wave-age interval resemble land conditions.

Figure 10 and Table III agree well with the experiments discussed above (e.g., van Atta and Chen, 1970; Paquin and Pond, 1971; Deacon, 1988). Low wave ages

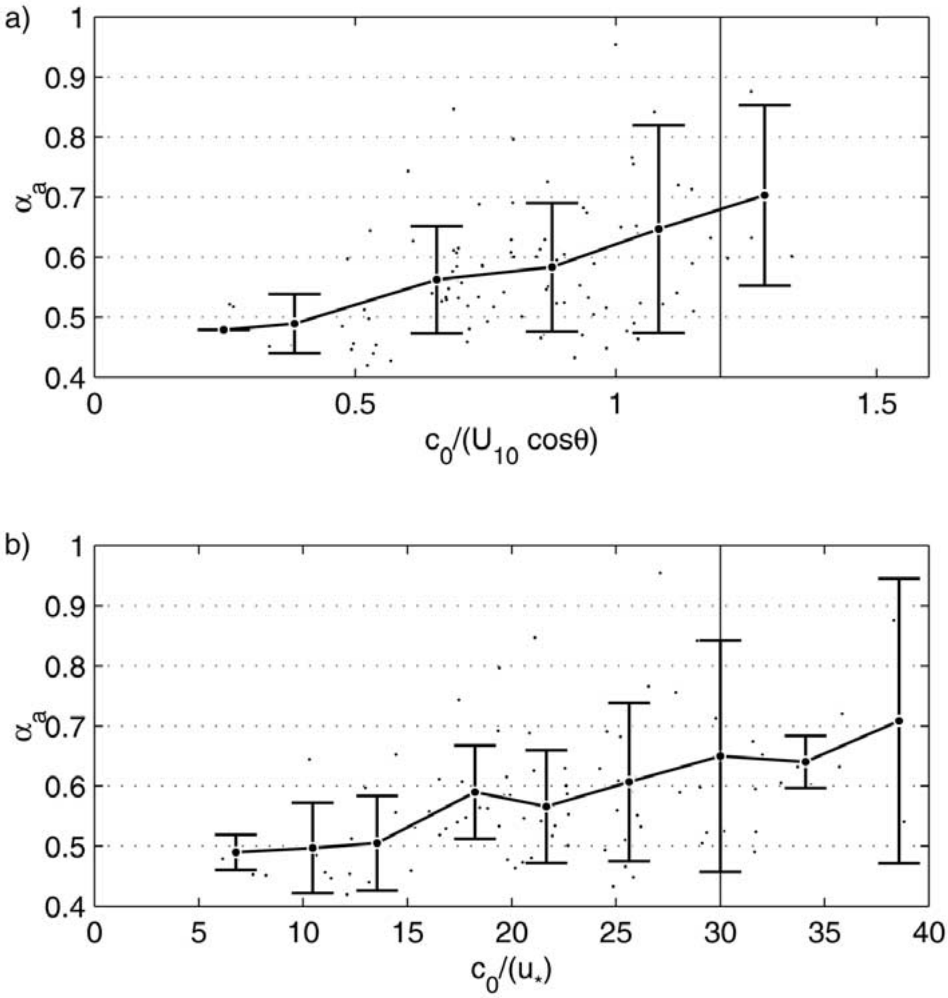

Figure 10. Effective values of the Kolmogrov constant, α_a, as a function of wave age: (a) $c_0/(U_{10}\cos\theta)$, (b) c_0/u_*. Symbols as in Figure 5. Very near-neutral data ($-0.01 < z/L < 0.01$).

(i.e., high wind speeds) have the lowest values ($\alpha_a \approx 0.48$), and high wave ages (i.e., low wind speeds) have the highest values ($\alpha_a \approx 0.70$). Even if a direct wave influence on α_a was not investigated in those experiments, an indirect influence can be found through the wind speed. It is also clear that the scatter in α_a found over sea is larger than over land (e.g., Deacon, 1988), which might indicate that earlier studies have been performed during different wave states.

6. Conclusions

It has been shown that a 'classical' form of IDM, with the assumption of zero imbalance, (i.e., that the sum of the transport terms is negligible) in the TKE budget, works reasonably well for average conditions. With a value of $\alpha_a = 0.55$ as an effective Kolmogorov constant, the mean relative difference between IDM and ECM is about 15% for the stability range $-1 < z/L < 0.5$, and about 10% for near-neutral conditions ($-0.02 < z/L < 0.02$). This is in accordance with, for example, Large and Pond (1981), who found good agreement between the two methods during near-neutral conditions.

The IDM method works best for high wind speeds and neutral conditions. For low wind speeds ($U < 6$ m s^{-1}) the relation between the two methods is more complex. IDM then gives higher values than ECM on average (about 20%), especially for swell conditions. The explanation is probably that the ϕ_m function used in the calculations is not valid over sea, and that no correction for the imbalance has been used.

For unstable conditions ($z/L < -2$) the main problem is how to determine the stability correctly. The bulk formulations used in the IDM gives too small values of $|z/L|$, since IDM do not seem to capture the wave influence, which reduces u_* to small values and produces large values of $|z/L|$. This will also be a problem when these erroneous values are used to derive the neutral drag coefficient C_{DN}.

The effective Kolmogorov constant α_a, which is designed to compensate for the imbalance between production and dissipation, seems to be a function of wave age, α_a increasing with increasing wave age. During saturated wave conditions ($0.5 < c_0/(U_{10} \cos\theta) < 1.2$ or $15 < c_0/u_* < 30$), the situation resembles land conditions (Sjöblom and Smedman, 2002) and a value of $\alpha_a = 0.59$ was found. This value was also suggested by Deacon (1988) for use over the sea.

In Sjöblom and Smedman (2003) it is shown by using the ECM that also the measurement height has to be taken into consideration. This means that the turbulent parameters not only have a dependence on the stability z/L, but an additional dependence on the actual height z itself, indirectly caused by the waves. When using IDM this also has to be accounted for in the parameterisation, implying that effectively different IDM algorithms have to be used for buoy measurements at a couple of metres above the water surface, and ship measurements at 10–30 m height.

To conclude, IDM works best for near-neutral conditions and high wind speeds, otherwise corrections have to be made depending on the wave age and wind speed, and probably a height dependence also has to be accounted for. An effective value of the Kolmogorov constant can therefore only be used if it is allowed to be a function of the above mentioned parameters.

Acknowledgements

This work has been performed within the EU-funded project AutoFlux (contract MAS3-CT97-0108). Dr. Margaret Yelland at SOC and Dr. Sophie Cloche at CETP are responsible for the inertial dissipation method calculations, and the authors would like to thank them for providing us with these invaluable data. The authors would also like to thank Dr. Hans Bergström and Dr. Mikael Magnusson for help with the eddy-correlation data and members of the MIUU staff for participation in the Östergarnsholm field campaigns. Dr. Kimmo Kahma and Dr. Heidi Pettersson at FIMR are acknowledged for the wave measurements and Barry Broman at SMHI for the sea-level measurements at Visby. Thanks are also given to Prof. em. Ulf Högström for valuable comments on the manuscript.

References

Anctil, F. and Donelan, M. A.: 1996, 'Air-Water Momentum Flux Observations over Shoaling Waves', *J. Phys. Oceanog.* **26**, 1344–1352.

Anderson, R. J.: 1993, 'A Study of Wind Stress and Heat Flux over the Open Ocean by the Inertial-Dissipation Method', *J. Phys. Oceanog.* **23**, 2153–2161.

Bergström, H. and Smedman, A.: 1994, 'Stably Stratified Flow in a Marine Atmospheric Surface Layer', *Boundary-Layer Meteorol.* **72**, 239–265.

Deacon, E. L.: 1988, 'The Streamwise Kolmogoroff Constant', *Boundary-Layer Meteorol.* **42**, 9-17.

DeCosmo, J., Katsaros, K. B., Smith, S. D., Anderson, R. J. Oost, W. A., Bumke, K., and Chadwick, H.: 1996, 'Air–Sea Exchange of Water Vapor and Sesible Hat: The Humidity Exchange over the Sea (HEXOS) Results', *J. Geophys. Res.* **101**, 12001–12016.

Donelan, M. A., Drennan, W. M., and Katsaros, K. B.: 1997, 'The Air–Sea Momentum Flux in Wind Sea and Swell', *J. Phys. Oceanog.* **27**, 2087–2099.

Drennan, W. M., Graber, H. C., and Donelan, H. C.: 1999, 'Evidence for the Effects of Swell and Unsteady Winds on Marine Wind Stress', *J. Phys. Oceanog.* **29**, 1853–1864.

Dupuis, H., Taylor, P. K., Weill, A., and Katsaros, K.: 1997, 'Inertial Dissipation Method Applied to Derive Turbulent Fluxes over the Ocean during the Surface of the Ocean, Fluxes and Interactions with the Atmosphere/Atlantic Stratocumulus Transition Experiment (SOFIA/ASTEX) and Structure des Echanges Mer-Atmosphere, Proprietes des Heterogeneites Oceaniques: Recherche Experimentale (SEMAPHORE) Experiments with Low to Moderate Wind Speeds', *J. Geophys. Res.* **102**, 21115–21129.

Edson, J. B., Fairall, C. W., Mestayer, P. G., and Larsen, S. E.: 1991, 'A Study of the Inertial-Dissipation Method for Computing Air–Sea Fluxes', *J. Geophys. Res.* **96**, 10689–10711.

Fairall, C. W., Edson, J. B., Larsen, S. E., and Mestayer, P. G.: 1990, 'Inertial-Dissipation Air–Sea Flux Measurements: A Prototype System Using Realtime Spectral Computations', *J. Atmos. Oceanic Tech.* **7**, 425–453.

Grachev, A. A. and Fairall, C. W.: 2001, 'Upward Momentum Transfer in the Marine Boundary Layer', *J. Phys. Oceanog.* **31**, 1698–1711.

Grelle, A. and Lindroth, A.: 1994, 'Flow istortion by a Solent Sonic Anemometer: Wind Tunnel Calibration and its Assessment for Flux Measurements over Forest and Field', *J. Atmos. Oceanic Tech.* **11**, 1529–1542.

Högström, U.: 1990, 'Analysis of Turbulence Structure in the Surface Layer with a Modified Similarity Formulation for Near Neutral Conditions', *J. Atmos. Sci.* **47**, 1949–1972.

Högström, U.: 1996, 'Review of Some Basic Characteristics of the Atmospheric Surface Layer', *Boundary-Layer Meteorol.* **78**, 215–246.

Josey, S. A., Kent, E. C., and Taylor, P. K.: 1999, 'New Insights into the Ocean Heat Budget Closure Problem from Analysis of the SOC Air-Sea Flux Climatology', *J. Climate* **12**, 2856–2880.

Kaimal, J. C. and Gaynor, J. E.: 1991, 'Another Look at Sonic Thermometry', *Boundary-Layer Meteorol.* **56**, 401–410.

Katsaros, K. B., Smith, S. D., and Oost, W. A.: 1987, 'HEXOS-Humidity Exchange over the Sea, A Program for Research on Water-Vapor and Droplet Fluxes from Sea to Air at Moderate to High Wind Speeds', *Bull. Amer. Meteorol. Soc.* **68**, 466–476.

Large, W. G. and Pond, S.: 1981, 'Open Ocean Momentum Flux Measurements in Moderate to Strong Winds', *J. Phys. Oceanog.* **11**, 324–336.

Large, W. G. and Pond, S.: 1982, 'Sensible and Latent Heat Flux Measurements over the Ocean', *J. Phys. Oceanog.* **12**, 464–482.

Maat, N., Kraan, C., and Oost, W. A.: 1991, 'The Roughness of Wind Waves', *Boundary-Layer Meteorol.* **54**, 89–103.

Oost, W. A., Fairall, C. W., Edson, J. B., Smith, S. D., Anderson, R. J., Wills, J. A. B., Katsaros, K. B., and DeCosmo, J.: 1994, 'Flow Distortion Calculations and their Application in HEXMAX', *J. Atmos. Oceanic Tech.* **11**, 366–386.

Paquin, J. E. and Pond, S.: 1971, 'The Determination of the Kolmogoroff Constants for Velocity, Temperature and Humidity Fluctuations from Second- and Third-Order Structure Functions', *J. Fluid. Mech.* **50**, 257–269.

Pierson, Jr., W. J. and Moskowitz, L.: 1964, 'A Proposed Spectral Form for Fully Developed Wind Seas Based on the Similarity Theory of S. A. Kitaigorodskii', *J. Geophys. Res.* **69**, 5181–5190.

Rieder, K. F. and Smith, J. A.: 1998, 'Removing Wave Effects from the Wind Stress Vector', *J. Geophys. Res.* **103**, 1363–1374.

Schacher, G. E., Davidson, K. L., Houlihan, T., and Fairall, C. W.: 1981, 'Measurements of the Rate of Dissipation of Turbulent Kinetic Energy, ϵ, over the Ocean', *Boundary-Layer Meteorol.* **20**, 321–330.

Sjöblom, A. and Smedman, A.-S.: 2002, 'The Turbulent Kinetic Energy Budget in the Marine Atmospheric Surface Layer', *J. Geophys. Res.* **107**(C10).

Sjöblom, A. and Smedman, A.-S.: 2003, 'Vertical Structure in the Marine Atmospheric Boundary Layer and its Implication for the Inertial Dissipation Method', *Boundary-Layer Meteorol.* **109**, 1–25.

Smedman, A., Högström, U., Bergström, H., Rutgersson, A., Kahma, K. K., and Pettersson, H.: 1999, 'A Case Study of Air–Sea Interaction during Swell Conditions', *J. Geophys. Res.* **104**, 25833–25851.

Smedman, A., Tjernström, M., and Högström, U.: 1994, 'The Near-Neutral Marine Atmospheric Boundary Layer with No Surface Shearing Stress: A Case Study', *J. Atmos. Sci.* **51**, 3399–3411.

Smith, S. D.: 1988, 'Coefficients for Sea Surface Wind Stress, Heat Flux, and Wind Profiles as a Function of Wind Speed and Temperature', *J. Geophys. Res.* **93**, 15467–15472.

Smith, S. D., Anderson, R. J., Oost, W. A., Kraan, C., Maat, N., DeCosmo, J., Katsaros, K., Davidson, K., Bumke, K., Hasse, L., and Chadwick, H. M.: 1992, 'Sea Surface Wind Stress and Drag Coefficients: the HEXOS Results', *Boundary-Layer Meteorol.* **60**, 109–142.

Taylor, P. K. and Yelland, M. J.: 2000, 'On the Apparent "Imbalance" Term in the Turbulent Kinetic Energy Budget', *J. Atmos. Oceanic Tech.* **17**, 82–89.

van Atta, C. W. and Chen, W. Y.: 1970, 'Structure Functions of Turbulence in the Atmospheric Boundary Layer over the Ocean', *J. Fluid Mech.* **44**, 145–159.

Volkov, Y. A.: 1970, 'Turbulent Flux of Momentum and Heat in the Atmospheric Surface Layer over a Disturbed Sea-Surface', *Izv. Acad. Sci, USSR Atmos. Oceanic Phys.*, *Engl. Transl.* **6**, 770–774.

Yelland, M. J. and Taylor, P. K.: 1996, 'Wind Stress Measurements from the Open Ocean', *J. Phys. Oceanog.* **26**, 541–558.

Yelland, M. J., Moat, B. I., Taylor, P. K., Pascal, R. W., Hutchings, J., and Cornell, V. C.: 1998, 'Wind Stress Measurements from the Open Ocean Corrected for Airflow Distortion by the Ship', *J. Phys. Oceanog.* **28**, 1511–1526.